JOURNAL OF GEOPHYSICAL RESEARCH, VOL. 115, B01102, doi:10.1029/2009JB006295, 2010

Tectonomagmatic activity and ice dynamics in the Bransfield Strait back-arc basin, Antarctica

Robert P. Dziak,[1] Minkyu Park,[2] Won Sang Lee,[2] Haru Matsumoto,[1] DelWayne R. Bohnenstiehl,[3] and Joseph H. Haxel[1]

Received 7 January 2009; revised 22 July 2009; accepted 2 September 2009; published 22 January 2010.

[1] An array of moored hydrophones was used to monitor the spatiotemporal distribution of small- to moderate-sized earthquakes and ice-generated sounds within the Bransfield Strait, Antarctica. During a 2 year period, a total of 3900 earthquakes, 5925 icequakes and numerous ice tremor events were located throughout the region. The seismic activity included eight space-time earthquake clusters, positioned along the central neovolcanic rift zone of the young Bransfield back-arc basin. These sequences of small magnitude earthquakes, or swarms, suggest ongoing magmatic activity that becomes localized along isolated volcanic features and fissure-like ridges in the southwest portion of the basin. A total of 122 earthquakes were located along the South Shetland trench, indicating continued deformation and possibly ongoing subduction along this margin. The large number of icequakes observed show a temporal pattern related to seasonal freeze-thaw cycles and a spatial distribution consistent with channeling of sea ice along submarine canyons from glacier fronts. Several harmonic tremor episodes were sourced from a large ($\sim$30 km^2) iceberg that entered northeast portion of the basin. The spectral character of these signals suggests they were produced by either resonance of a small chamber of fluid within the iceberg, or more likely, due to periodicity of discrete stick-slip events caused by contact of the moving iceberg with the seafloor. These pressure waves appear to have been excited by abrasion of the iceberg along the seafloor as it passed Clarence and Elephant Islands.

Citation: Dziak, R. P., M. Park, W. S. Lee, H. Matsumoto, D. R. Bohnenstiehl, and J. H. Haxel (2010), Tectonomagmatic activity and ice dynamics in the Bransfield Strait back-arc basin, Antarctica, *J. Geophys. Res.*, *115*, B01102, doi:10.1029/2009JB006295.

1. Introduction

[2] The Bransfield Strait is geographically located between the South Shetland Islands and western Antarctic Peninsula, in an area of evolving tectonics driven by the interaction of the Antarctic, Scotia, and South American plates (Figure 1). The Bransfield Strait seafloor is a Quaternary back-arc basin and is one of only two back-arc basins forming in continental crust that are opening without a large strike-slip component [*Lawver et al.*, 1996]. Fresh volcanic rocks occur on numerous submarine features distributed along the rift axis, including a discontinuous neovolcanic ridge similar to the nascent spreading centers seen in some other back-arc basins.

[3] For the first time, an array of moored hydrophones was deployed within the Bransfield Strait, with 7 instruments from December 2005–2006 and 6 instruments from 2006 to December 2007. The hydrophones record the acoustic Tertiary (*T*) waves of subseafloor earthquakes that propagate in the ocean water column, primarily as surface-related phases at these high southern latitudes (Figure 2). Using regional *T* waves to detect submarine earthquakes typically provides a complete catalog of $\geq$3.0 m_b earthquakes from remote ocean basins [*Dziak et al.*, 2004], a significant improvement over the $\sim$4.5 m_b detection limit of land-based seismic networks for the southern ocean. In addition to seismoacoustic signals, the hydrophones record the broadband arrivals of ''icequakes'' that result from cracking, collision, and breakup of icebergs, ice flows and ice sheets within and along the periphery of the strait. The goal of this study is to use hydrophone recorded seismicity to provide insights into the style of rifting (volcanic versus tectonically dominated) along the Bransfield seafloor back-arc rift zone, identify centers of recent magmatic activity within the back-arc basin, and evaluate the meteorological or possible geophysical processes influencing icequakes (breakup) in the region.

2. Tectonic and Volcanic Setting

[4] The seafloor of the Bransfield Strait is a northeast trending, ensialic back-arc basin at the transition from rifting to spreading [*Keller et al.*, 2002; *Christeson et al.*, 2003;

[1]Cooperative Institute for Marine Resources Studies, Oregon State University, NOAA Newport, Oregon, USA.
[2]Polar Environmental Research Division, Korea Polar Research Institute, Incheon, South Korea.
[3]Department of Marine, Earth and Atmospheric Sciences, North Carolina State University, Raleigh, North Carolina, USA.

0148-0227/10/2009JB006295$09.00

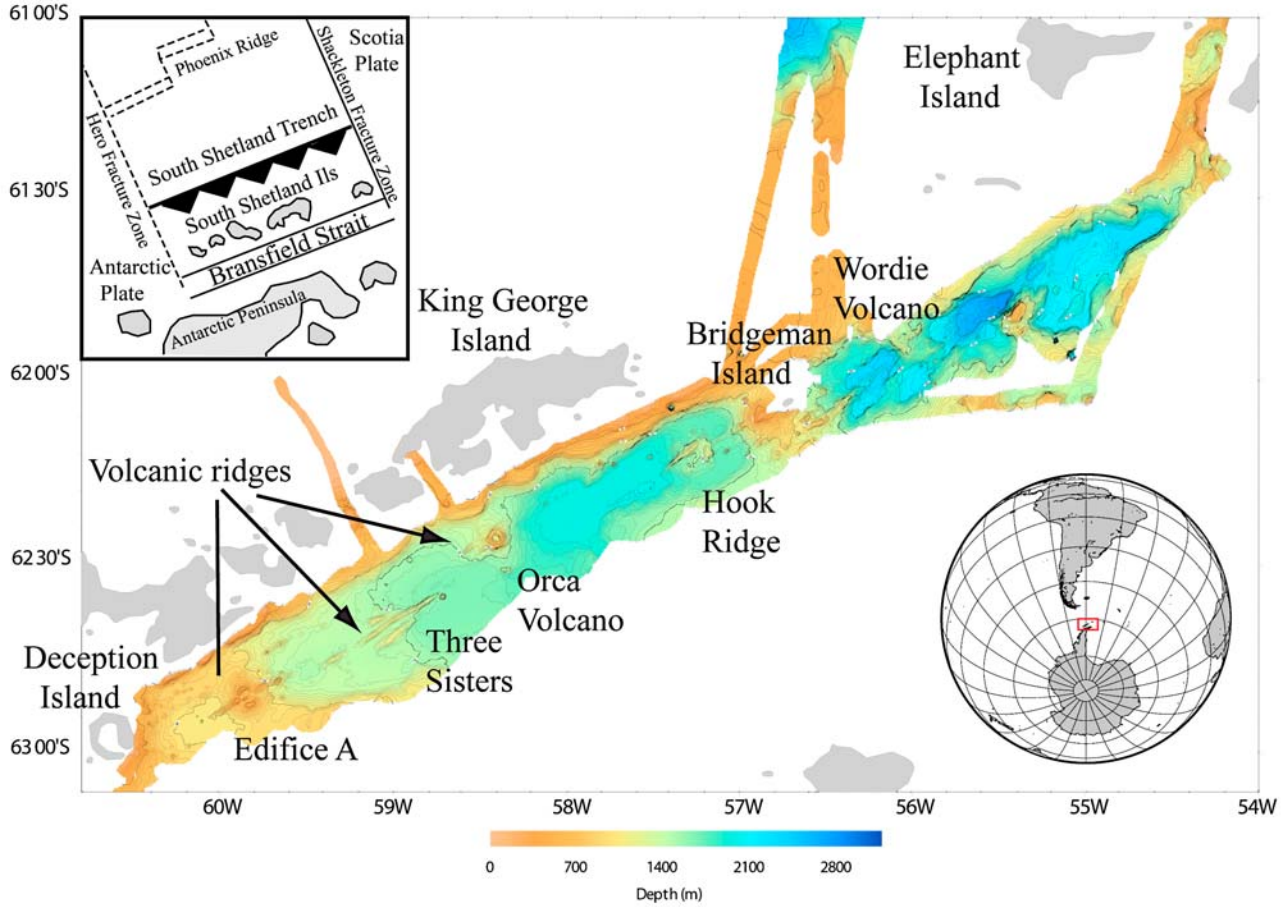

Figure 1. Bathymetric map of Bransfield Strait and Drake Passage, along the west coast of the Antarctic Peninsula [*Lawver et al.*, 1996]. Names of major volcanic centers and significant islands are labeled. The "neovolcanic" zone of the Bransfield back-arc spreading center is the elongate bathymetry in the center of basin. Inset map shows a simple tectonic map of the region. The Phoenix Ridge and Hero Fracture Zone are currently extinct, with rollback of the slab at the trench leading to back-arc extension.

Grad et al., 1992, 1997]. Extension is a result of either slowly continuing subduction and rollback of the Phoenix Plate beneath the South Shetland island arc (Figure 1) or simple shear between the Scotia and Antarctic Plates [*Barker and Austin*, 1998; *González-Casado et al.*, 2000; *Lawver et al.*, 1996; *Maestro et al.*, 2007; *Robertson-Maurice et al.*, 2003]. The central Bransfield back-arc rift basin has a crustal thickness of at least 9 km [*Christeson et al.*, 2003; *Grad et al.*, 1997] and has a broad axial zone of recently or currently active seamounts and volcanic ridges (Figure 1) [*Gràcia et al.*, 1997; *Lawver et al.*, 1996]. Fresh volcanic rocks occur on many of these submarine volcanic features distributed along the rift axis, including a discontinuous neovolcanic ridge similar to spreading centers seen in other, nascent back-arc basins [*Keller et al.*, 2002]. Smaller edifices near the northeast end of the rift yield basalts with arc-like compositions whereas the most mid-ocean ridge-like basalts are from a large, caldera-topped seamount and a 30-km-long axial neovolcanic ridge toward the southwest end of the rift, but these two features also yield lavas of andesitic and rhyolitic compositions, respectively. The along-axis bathymetric deepening of the central Bransfield back-arc basin, the basin morphology, form of volcanic extrusion and progressive crustal thinning have been attributed to rift propagation from NE to SW along the basin axis [*Barker and Austin*, 1998; *Barker et al.*, 2003; *Christeson et al.*, 2003]. High-temperature hydrothermal signatures also have been observed in the water column of the Bransfield Strait [*Klinkhammer et al.*, 2001; *Keller et al.*, 2002] indicative of underlying volcanic activity in this slow spreading region.

[5] Extensional structures along the South Shetland Islands margin are composed of a few closely spaced large offset normal faults, whereas the Bransfield back-arc rift zone adjacent to the Antarctic Peninsula exhibits broader, distributed extension and no magmatism [*Barker and Austin*, 1998; *Barker et al.*, 2003]. Normal faulting of arc crust [*Barker and Austin*, 1998; *Prieto et al.*, 1998] suggests that the Bransfield back arc, like the western Woodlark Basin in the western Pacific, is in transition from intra-arc rift to ocean basin [*Taylor et al.*, 1999] where initial extension and magmatic inflation are followed by deflation and collapse along intracrustal detachments [*Barker and Austin*, 1998]. Additionally, ice flows have modified the bathymetry of the Bransfield back-arc basin, with major erosional and depositional features on the basin floor associated with past ice flow during the Last Glacial Maximum (from the Antarctic Peninsula)

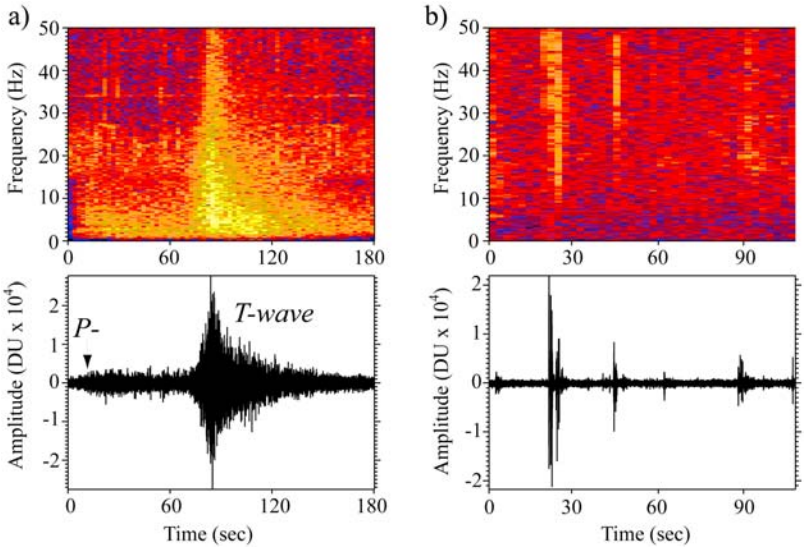

Figure 2. Time series and spectrogram of hydrophone data (station 5) examples of an earthquake (a) and icequake (b) acoustic arrivals. The earthquake shown occurred on 5 April 2007 and was a 4.7 m_b event that occurred at the southwest Bransfield Strait (event mechanism within box in Figure 3). Earthquakes produce seismic phases that covert to an acoustic phase at the seafloor-ocean interface. This acoustic earthquake phase propagates laterally through the water column as a broadband (3–50 Hz) arrival referred to as a *T* wave. The faster direct P wave arrival is also recorded by the hydrophone as a locally converted acoustic phase. Icequakes originate in sea surface ice and produce acoustic phases that propagate solely in the water column downward toward the hydrophone. Icequakes arrivals are distinguished from earthquakes by their impulsive, short-duration coda (~10 s) and higher-frequency content (>10–50 Hz).

identified along the southeastern margin [*Canals et al.*, 2000, 2002]. The grounding line in the east central Bransfield back-arc basin during the Last Glacial Maximum is estimated at 400 m depth [*Banfield and Anderson*, 1995].

[6] Figure 3 shows the 14 centroid moment tensor solutions available for this region from 1976 to 2008 (Global CMT Project, http://www.globalcmt.org); these events range in magnitude from 5.0 to 6.0 m_b. The mechanisms show predominantly strike-slip motion along the Shackleton Fracture Zone, normal fault motion at the southwest Bransfield back arc (southwest of Deception Island), and single thrust and normal fault events near Elephant Island, South Shetland Islands and Trench. More recent local seismic studies [*Robertson-Maurice et al.*, 2003] recorded a total of 150 small magnitude (2–5 m_b) earthquakes over a 6 month period from throughout the region. These local events exhibited six normal faulting mechanisms at the back arc, one thrust event at the trench, and a small group of five earthquakes at a submarine volcano suggesting recent magmatic activity.

[7] If subduction is still occurring beneath the South Shetland Islands, the subduction rate should be similar to the opening rate of the Bransfield back arc, as there is no relative motion between the subducting plate and the Antarctic Peninsula. GPS measurements indicate a spreading rate of ~1 cm yr^{-1} or slower [*Bevis et al.*, 1999; *Dietrich et al.*, 2001], which suggests the South Shetland Trench represents an extreme end-member of hot subduction involving slow convergence of young (14–23 Ma) oceanic lithosphere. With cessation of spreading along the Phoenix Ridge at ~4 Ma, this slow subduction is thought to be driven by the "rollback" of the trench caused by the vertical subsidence of the slab into the upper mantle [*Lawver et al.*, 1996]. Thus extension in the southwest Bransfield back arc is initiated by rollback as a slab window opened, whereas extension in the northeast may be augmented by left-lateral transtension from reorganization of the Shackleton Fracture Zone–Scotia Ridge intersection [*Barker and Austin*, 1998].

3. Bransfield Seismicity

[8] From December 2005 to December 2007, a total of 3,146 earthquakes were located in the Bransfield back-arc basin, and another 754 earthquakes were located throughout the region including the South Shetland Trench and Drake Passage (Figures 3 and 4). Bransfield earthquakes locate throughout the basin and along the neovolcanic zone of the back-arc spreading center. The hydroacoustically determined source locations were estimated using an iterative nonlinear regression algorithm that minimizes the error between observed and predicted travel time by incrementing an event's latitude, longitude, and origin time. Travel times and velocities along acoustic paths are estimated by applying propagation models to the U.S. Navy ocean sound-speed database, the Generalized Digital Environmental Model [*Davis et al.*, 1986]. The sound propagation field in the Bransfield Strait water column is surface limited, meaning sound velocity decreases linearly from the seafloor to the sea surface (Figure 5). This causes all rays from both seafloor and shallow water sources to turn up toward the sea

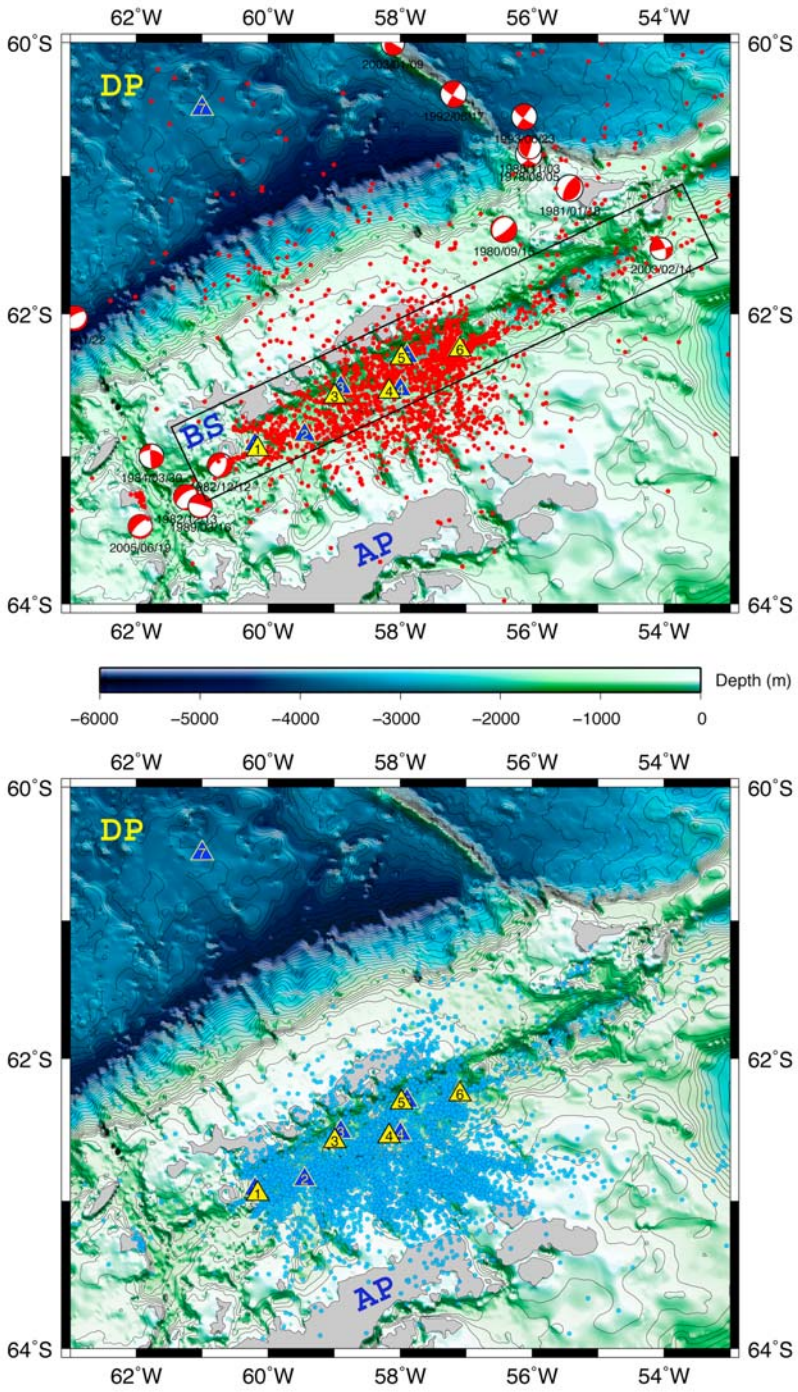

Figure 3. (top) Earthquakes and (bottom) icequakes located using the hydrophone arrays during the 2 year deployment. Blue and yellow triangles represent for 2005–2006 hydrophone mooring deployments (seven instruments) and 2006–2007 deployments (five instruments), respectively. Only five hydrophones were used to estimate locations from 2005 to 2006 data due to clock errors (see Figure 4). Labels indicated the Drake Passage (DP), Bransfield Strait (BS), and Antarctic Peninsula (AP). Box shows earthquakes used to create Figure 5. Bathymetry is from *Sandwell and Smith* [1997] satellite altimetry. Red focal mechanisms show the 14 Harvard centroid moment tensor solutions that were determined for this region from 1976 to 2008. Earthquakes range in magnitude from 5.0 to 6.0 m_b, showing strike-slip motion along the Shackleton Fracture Zone and normal fault motion at the southwest Bransfield basin. The most recent CMT solution is for an earthquake that occurred in June 2005, prior to the hydrophone deployment.

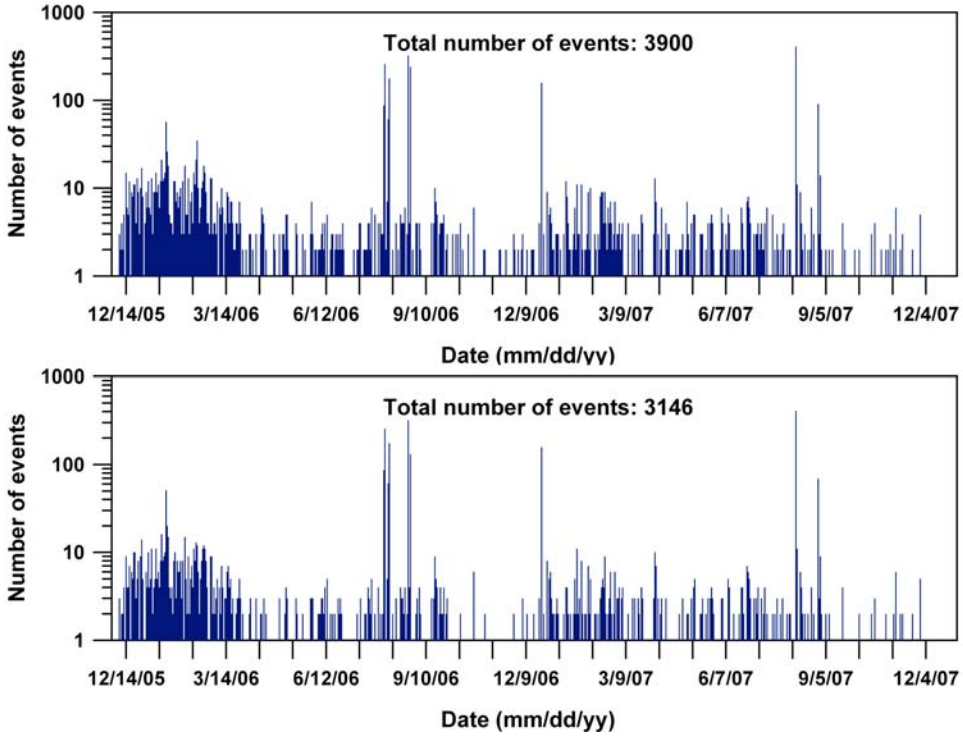

Figure 4. (top) Histogram of total number of hydroacoustic earthquakes from the entire region and (bottom) histogram of events within the Bransfield Strait (earthquake counts are from box in Figure 1). Bransfield seismicity dominates the number of earthquakes, with only 754 total events being recorded from outside the Bransfield.

surface and then propagate laterally through multiple reflections from the sea surface, and possibly seafloor.

[9] Accurate ocean sound speed models and good azimuthal distribution of the autonomous hydrophone array relative to the Bransfield back arc allows for well-constrained earthquake locations. Event location error is available as output from the regression algorithm covariance matrix [*Bevington and Robinson*, 1992], with the range in location error within the array aperture of ±0.5–5 km in latitude and longitude at the 68% confidence interval (Figure 6). Location error increases outside of the array, being ±10–20 km in latitude and longitude along the Antarctic Peninsula and South Shetland Trench. The peak amplitude near the center of the earthquake acoustic signal packets (commonly referred to as the "*T* wave") is typically selected as the arrival time of the earthquake for location purposes, since it corresponds to the high-energy phases radiated from nearest the epicentral region [*Slack et al.*, 1999]. Although earthquake acoustic locations are well constrained, earthquake focal depth and source parameter information are not currently available from our hydroacoustic analysis techniques.

[10] An acoustic magnitude, or source level (SL), is calculated for each earthquake by removing the effects of geometric spreading along the propagation path and the hydrophone instrument response [*Dziak*, 2001]. Source levels for Bransfield back-arc earthquakes range from 170.8 to 234.1 dB (dB), where dB is relative to 1 μPa (pressure) at 1 m. There were no teleseseismically recorded earthquakes from the Bransfield during 2005–2007 to allow for a robust estimate of seismic to acoustic magnitude relationships; however, seismic magnitudes of the Bransfield earthquakes can be estimated using an empirical source level to body wave magnitude (m_b) relationship developed for the north Atlantic hydrophone array of SL = 18.95 m_b + 151.91 [*Dziak et al.*, 2004]. This equation provides an estimate of magnitude range for Bransfield events of 1.0–4.4 m_b, where the magnitude of completeness is 208 dB or 3.0 m_b (Figure 7). Since none of these hydroacoustic events were recorded on global, land-based seismic networks, this implies a >4.4 m_b earthquake detection threshold for the Bransfield–South Shetland Island region.

[11] The levels of continuous background seismicity vary through the 2 year experiment, with long-term peaks in activity observed from December 2005 to March 2006 and December 2006 to October 2007. The majority of seismicity also appears to be spatially limited along the back arc to within the 225 km distance between Deception and Bridgeman Islands (Figure 3). Given that the rift basin extends beyond Elephant Island (Figures 1 and 3), significant earthquake activity might be expected to the northeast of the array. The dearth of events to the east of Bridgeman Island therefore may in part reflect locally increasing location errors and higher detection thresholds (Figure 6).

[12] There also appear to be eight distinct spatiotemporal clusters, or swarms, of seismicity along the neovolcanic zone of the back arc. All eight earthquake swarms occurred at, or along the flanks of, major volcanic centers within the back-arc basin (Figure 8) implying the seismicity was caused by magmatic activity (as argued by *Robertson-Maurice et al.* [2003]), in that although the earthquakes may be caused by "tectonic" slip on a fault, the fault slip is likely occurring because magma is moving at depth in the crust beneath the

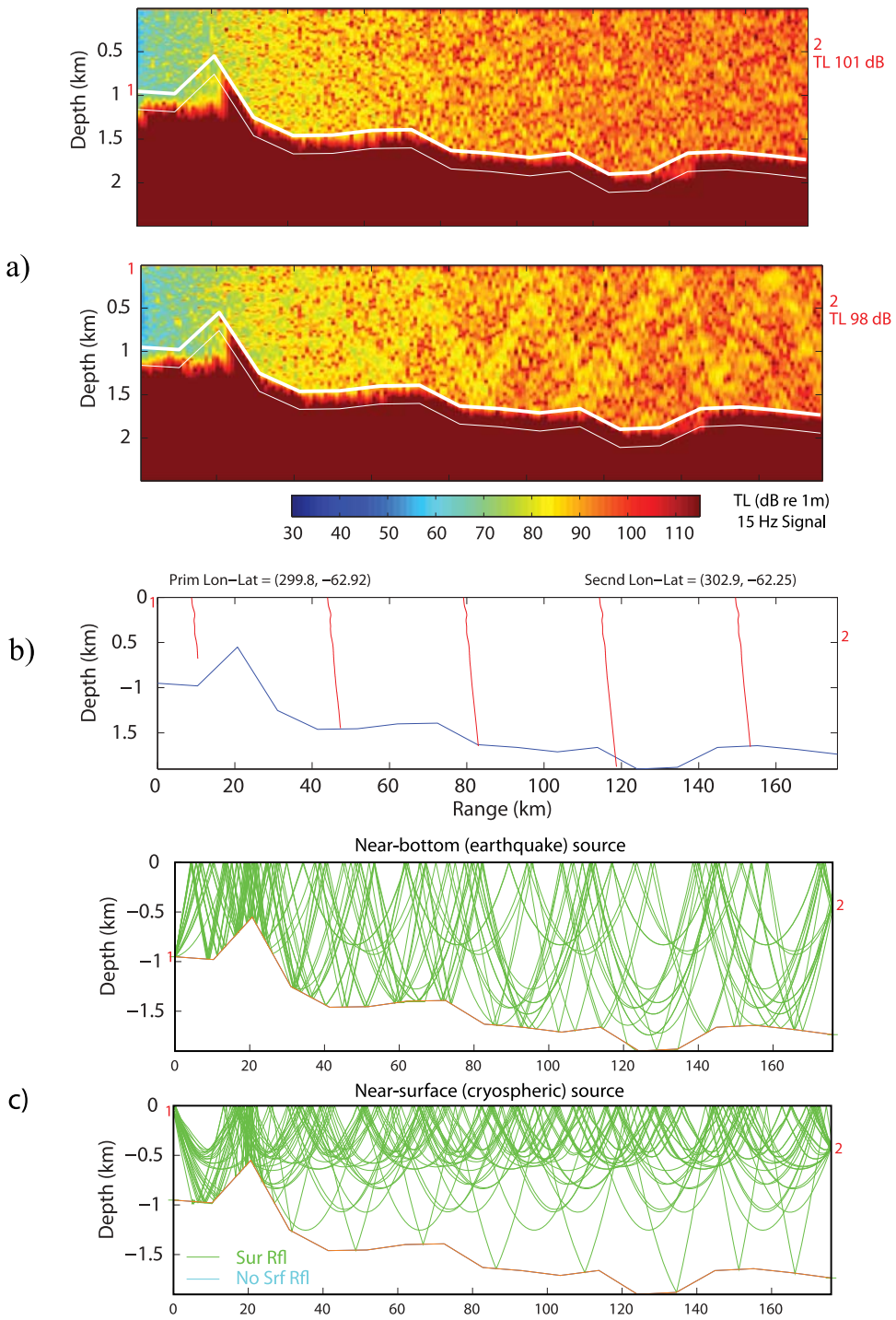

Figure 5. (a) The acoustic propagation loss models and (c) acoustic ray trace models for near-surface and seafloor sources from southwest to northeast between hydrophones 1 and 6 [*Dushaw and Colosi*, 1998]. Ray trace model used subhorizontal takeoff angles ±12.5°. (b) Sound speed profiles along the Bransfield Strait shown via red lines and derived from the annual WOA05 climatology, which is essentially range-independent at <1° distances. Models demonstrate the larger amount of bottom interaction associated with the seafloor propagation from an earthquake source. Both seafloor and shallow source scenarios show clear propagation across the length of the basin with modest transmission loss at the hydrophone depths of 500 m.

surface faults. The swarms occurred at (in temporal order) Hook Ridge, Three Sisters, Edifice-A, Bridgeman Island, Wordie Volcano, Orca Volcano, Three Sisters, and Deception Island. The three earthquake swarms at Edifice-A and Three Sisters show some indication of earthquake migration, which is observed during magma injection events at mid-ocean ridges [*Dziak et al.*, 2007]. However, the apparent direction of earthquake propagation is oblique to the strike of the rift

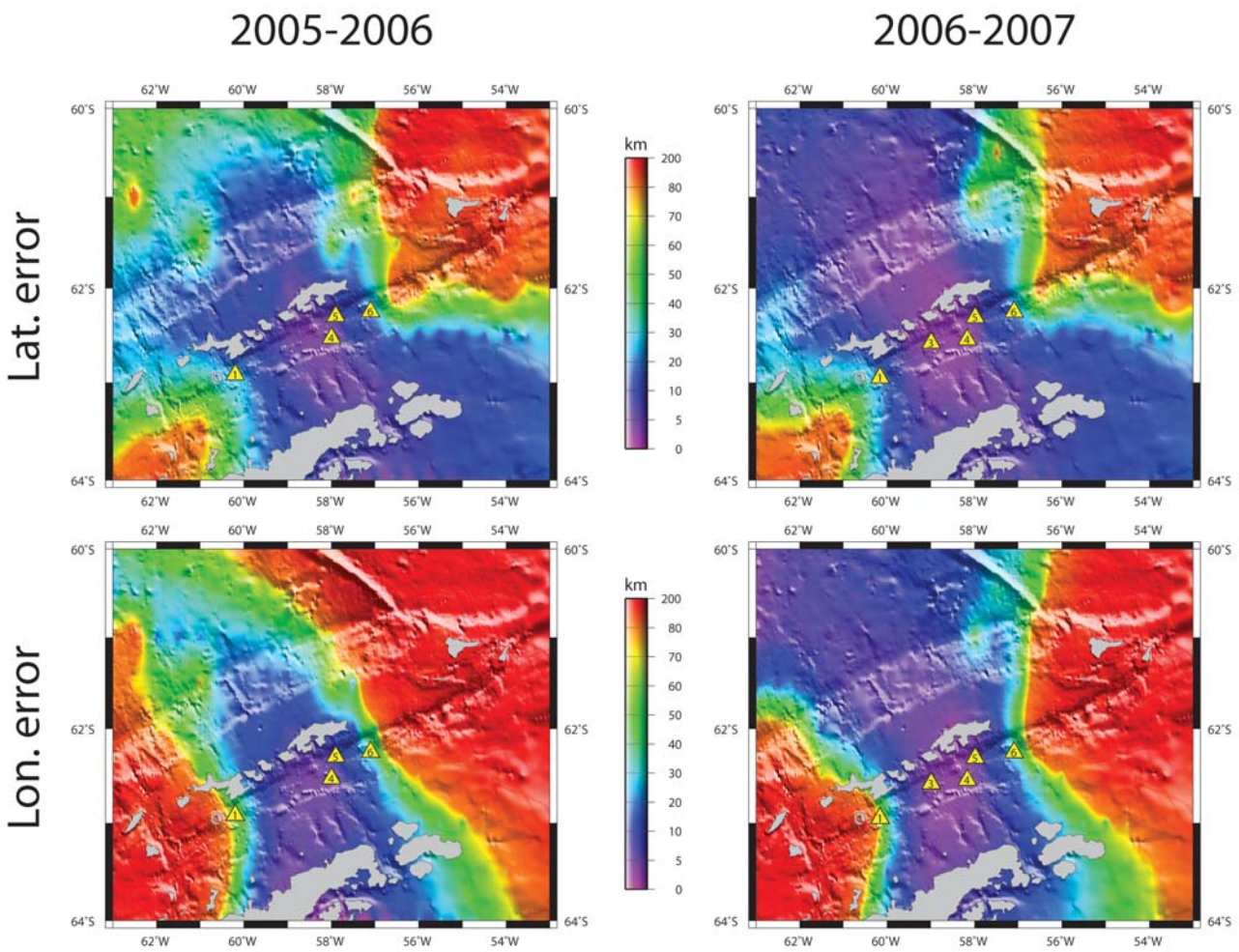

Figure 6. Simulated location errors (km with 68% confidence limits) in (top) latitude and (bottom) longitude for the hydrophone array geometry in the Bransfield Strait. A normally distributed 0.5 s pick error has been introduced to all arrivals at the hydrophones. A total of 100 simulations were run at each 0.25° node. Estimated errors range from 0.5 to 5.0 km in latitude and longitude within the array and increase to 10–20 km in latitude outside the array aperture.

zone, and given the location error, the epicenter migration may not be statistically significant. Moreover, the obliquity of the earthquake locations for the August 2006 Three Sisters and Hook Ridge swarms is due to the two-dimensional location error of the hydroacoustic techniques, where epicenters follow common travel time hyperboles because many of the events are very small magnitude and reliable selection of phase arrival times is more difficult. In these cases, the true location of the swarm events is the likely the centroid of the swarm cluster, where event locations distribute out 1σ distance (±10–20 km error) from the swarm center. The five other earthquake swarms remained equidistant from the nearest volcanic center during the duration of activity, implying that magma was not injected laterally along the rift zone during these episodes. It also is interesting to note that four of the swarms occurred during a three-week period in August 2006 (Figure 8). In total these four swarms are distributed over nearly the entire 400 km length of the Bransfield back-arc rift, from Deception Island to Wordie Volcano. This also represents the only time during the experiment when significant seismicity was observed in the section of the rift between Wordie Volcano and the intersection with the Shackleton Fracture Zone.

[13] In addition to the Bransfield rift-related seismicity, the hydrophone array detected a large amount of seismicity along the northern and southern margins of the Bransfield back-arc basin, as well as 122 earthquakes from the South Shetland Trench (Figure 3). The margin events are likely related to normal fault processes due to back-arc extension. The earthquakes ocean ward from the South Shetland Islands implying there is active, gravity-driven subduction beneath the South Shetland Islands. Since the Phoenix Ridge is extinct and the slab is not actively converging, subduction seismicity is being driven by the slab rollback processes. However, with the lack of focal depth and fault parameter information from the hydroacoustic it is not clear where in the slab and what exact slab deformation process is involved in producing the trench earthquakes.

[14] The possible correlation of Bransfield back-arc seismicity with tidal stresses also was investigated. The triggering of microearthquakes ($M_L < 2$) at spreading centers due to the removal of vertical loads (ocean tidal loading) [*Wilcock*,

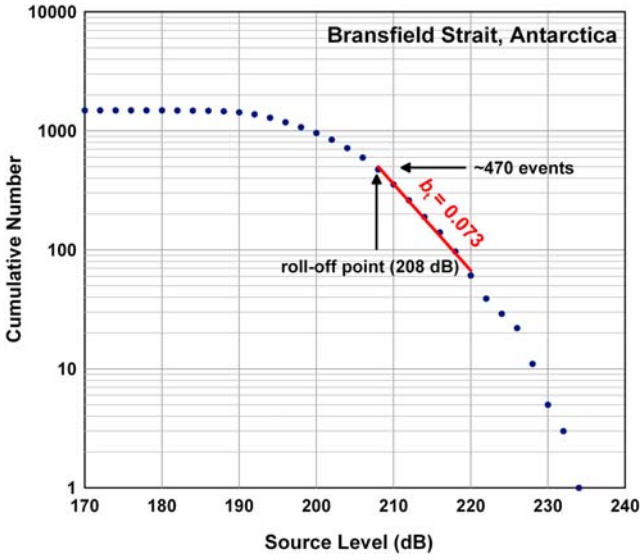

Figure 7. Diagram of cumulative number of earthquakes versus the earthquake source level (dB = 1 μPa at 1 m). Source level represents acoustic magnitude of each event. Significant earthquake swarms were removed from the hydroacoustic earthquake database (declustered) following the method of *Stroup et al.* [2007], prior to plotting of this relationship. Source levels for Bransfield earthquakes range from 170.8 to 234.1 dB, which relates to a seismic magnitude detection range of 1.0–4.4 m_b for Bransfield events. The magnitude of completeness is 208 dB, roughly equivalent to a 3.0 m_b.

2001; *Tolstoy et al.*, 2002] or the direct solid Earth tide [*Stroup et al.*, 2007] has been demonstrated in previous studies. We calculated the ocean tidal load and solid Earth tide using the GOTIC2 model of *Matsumoto et al.* [2001]. Time series representing the tidal sea surface height (maximum of 1 m) and tidally induced stress changes (maximum of 20 kPa) were cross correlated with that of the Bransfield seismic database, both before and after catalog declustering. No statistically significant correlation was found, indicating that the nucleation of small-to-moderate magnitude earthquakes along the Bransfield fault systems is insensitive to semidiurnal stress change of this magnitude. By contrast, the timing of microearthquake cracking events of a hydrothermal origin has been shown to be modulated by volumetric stress changes as small as 1 kPa [*Stroup et al.*, 2007]. This presumably reflects higher rates of stressing within the hydrothermal reaction zone and consequently shorter earthquake nucleation times that respond to these short-period tidal stress changes [*Stroup et al.*, 2007].

4. Bransfield Icequakes and Iceberg Tremor

[15] Icequakes are impulsive, broadband, short-duration (<30 s) signals with dominant energy in the 40–125 Hz band, in contrast to earthquake generated *T* waves that exhibit energy over the 1–50 Hz band (Figure 2). Icequakes may be caused by thermal stresses, as well as physical deformation of the ice from wind, currents, waves and collisions. These external forcing factors result in shear failure of the ice crystal lattice, generating pressure waves that emanate into the water column.

[16] A total of 5,925 icequake locations were derived from the hydrophone data set (Figure 9). The icequake locations (Figure 3, bottom) parallel the coast of the Antarctic Peninsula, and are distributed throughout the waters of the Bransfield Strait. The icequake locations along southeast of the Bransfield Strait also separate into six lobes that trend toward the Antarctic Peninsula. These lobes are not interpreted as artifacts of the location algorithm, since they are perpendicular to the error surface and exceed location error (Figure 6). Notably, they appear to parallel the trends of submarine canyons, suggesting that sea ice may accumulate in areas of glacial outflow. A similar correlation between ice tremor and outlet glaciers has been noted for the Wilkes Land coast [*Chapp et al.*, 2005].

[17] The number of icequakes recorded varies regularly with season, with more events being detected during the austral summer months (Figure 9). Autocorrelation of icequake activity indicates that the correlation has a maximum value at a lag of 207.3 days, with other peaks at 103.6 and 310.9 days. This is consistent with an approximately 6 month seasonal periodicity, which likely reflects variable thermal and wind stress conditions during the annual freeze-thaw cycle.

[18] The possible correlation of Bransfield icequakes with ocean and solid Earth tidal stresses and sea surface tidal height also was investigated. As with the earthquake data, no statistically significant correlation was found between tides and icequakes.

[19] Another remarkable cryogenic sound recorded on the hydrophone array was produced by the grounding and subsequent movement of large icebergs along the Bransfield seafloor (Figure 10a). The sliding of the iceberg along the seafloor, caused by a combination of winds and ocean currents, produces pressure waves that enter and resonate in the iceberg, presumably in discrete zones that are a quasi-liquid/crystal bounded by an impedance contrast with the remaining frozen portion of the iceberg. Thus these signals differ significantly from the icequakes, which correspond to the failure of cracks in the ice. Iceberg tremor was recorded on the Bransfield hydrophone array in January 2006 and July–August 2006. The fundamental frequency of the tremor is between 40 and 50 Hz, with as many as 5 overtones at ~16 Hz integer spacing observed up to the filter cutoff of 125 Hz. This signal bandwidth places it within the upper frequency range of ice-generated tremor signals previously recorded, where tremor from large (>10 km) icebergs from other regions of Antarctica has been shown to exhibit signals with a fundamental frequency typically between 2 and 10 Hz [*Talandier et al.*, 2002; *Chapp et al.*, 2005; *MacAyeal et al.*, 2008]. The phenomenon of "gliding" is also visible in the spectrogram where the packet of ensemble spectral peaks varies in frequency through time while maintaining their harmonic spacing [*Garces et al.*, 1998], giving the signals a unique spectral character. We were able to use the August 2006 tremor signals to locate their source, which corresponded to a large (>10 km long) iceberg in the waters of the northern Bransfield Strait region, identified and named from satellite images as UK213 (Figure 10b). It is very doubtful these harmonic signals are from the propellers of

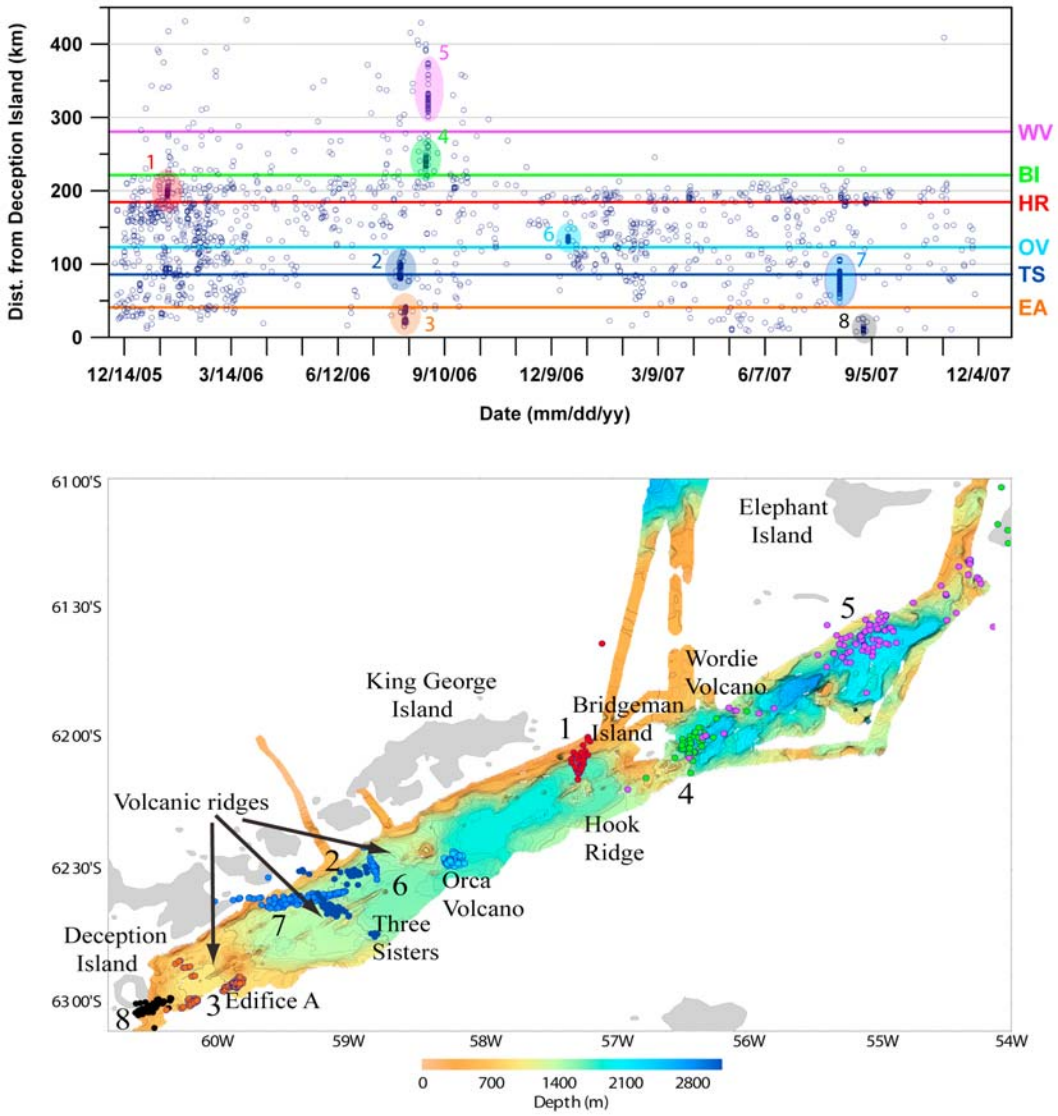

Figure 8. (top) Diagram of distribution in time and distance of hydroacoustic earthquake locations. The time axis is the entire 2 year hydrophone deployment, distance is in km uprift along Bransfield neovolcanic zone, with Deception Island as the reference point. (bottom) Earthquakes with temporal clustering in eight distinct swarms occurring at the volcanic centers, with each earthquake cluster color coded to appropriate volcanic center. Swarms are numbered by date of occurrence. The major Bransfield seafloor volcanoes are labeled and triangles give their locations: EA, Edifice-A volcano; TS, Three Sisters; OV, Orca Volcano; HR, Hooks Ridge; WV, Wordie Volcano. Figure 8 (bottom) shows map view distribution of earthquake swarm in relation to volcanic centers.

passing ships or cetacean vocalizations, since the iceberg tremor signals are very high energy sources and arrive on all hydrophones. Ships and cetacean species typically do not produce sound at high enough energy levels to be recorded across a 400 km aperture array.

5. Discussion

[20] Overall, the hydroacoustic earthquake data show the Bransfield back-arc basin to be a seismically active region, with both the central seafloor rift zone and surrounding basin margins producing thousands of earthquakes during the 2 year recording period. The Bransfield Strait region also exhibits thousands of icequakes and other cryogenic sound sources and clearly is an area of dynamic sea ice activity. Histograms of Bransfield back-arc earthquake and water column icequake counts indicate both have a seasonal pattern, where icequakes and earthquakes peaking in austral summer and spring and exhibit the lowest levels during the winter. The temporal variability of icequakes, with a periodicity of 207 days, can be related to seasonal freeze-thaw and wind stress cycles. A mechanism to explain the temporal distribution of earthquakes is less clear. As no significant tidal or seasonal influence on Bransfield back-arc seismicity has been found, the observed pattern may simply be coincidental.

[21] The Bransfield back-arc basin exhibits both steady state seismicity as well as spatiotemporal clustering into

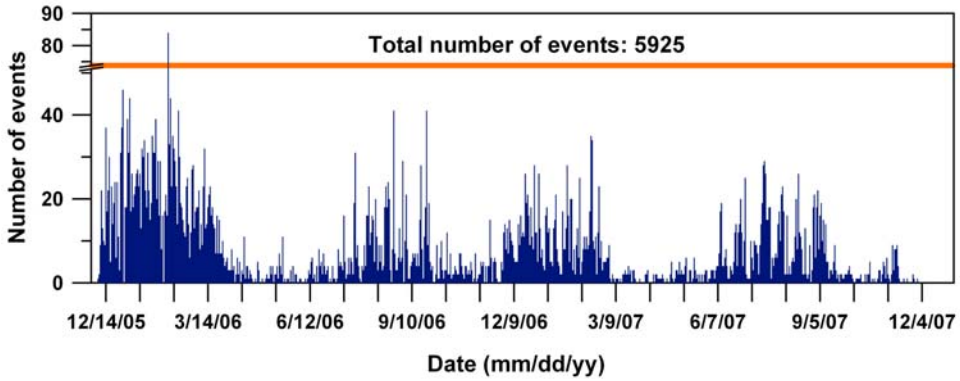

Figure 9. Histogram showing total number of hydroacoustic icequakes recorded from the entire region and within the Bransfield Strait. Regional icequakes show a strong seasonal occurrence rate with the austral summer-spring seasons showing peaks in icequake activity. Autocorrelation shows a maximum correlation at 207.3 days periodicity consistent with a 6 month seasonal variation in icequake activity related to thermal and wind stresses due winter-summer freeze-thaw cycles.

distinct earthquake swarms that are localized near major volcanic centers. First-order analysis of the spatial distribution in seismicity implies the 225 km section of back-arc rift between Deception and Bridgeman Islands is in an active seismic phase that exhibits several month long periods of increased and decreased activity. While significant steady state earthquake activity might be expected past Bridgeman Island, given the rift extends to near Elephant Island where it intersects the Shackelton Fracture Zone, the lack of earthquakes in this section is probably a result of increased location error due to the hydrophone array geometry. However, the presence of the two August 2006 earthquake swarms on the rift northeast of Bridgeman does imply this section of the back arc experiences rifting during brief periods (hours to days) of intense earthquake activity. Moreover, the earthquake swarms northeast of Bridgeman

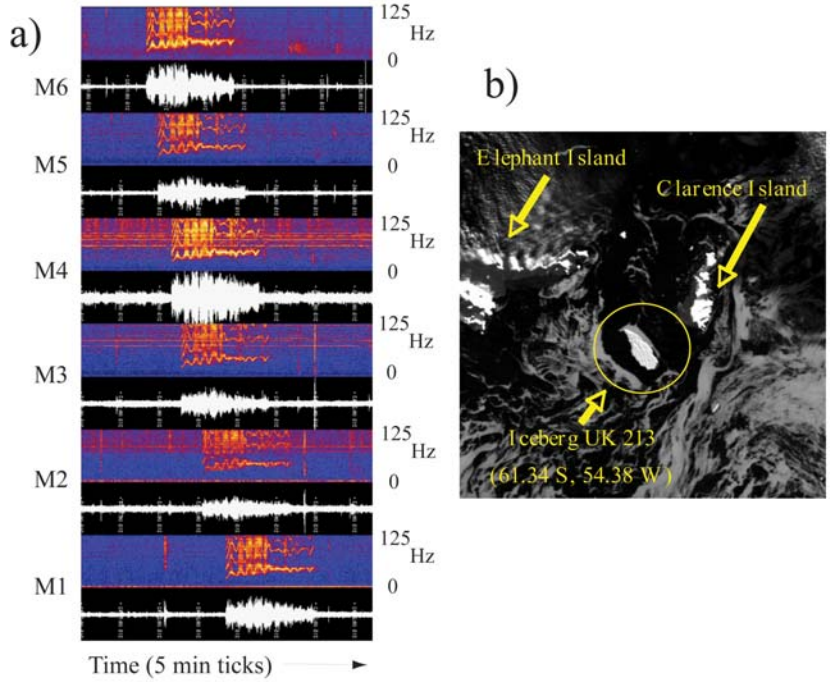

Figure 10. (a) Time series and spectrogram of hydrophones M1–M6 showing iceberg tremor records arrivals. The onset of tremor was used as arrival times to derive location shown in Figure 10b. (b) Location corresponding to Iceberg UK213. Satellite image is from the U.S. National Snow and Ice Data Center, sunlight angle is from the northeast. The tremor record has a fundamental of between 40 and 50 Hz with a total of five overtones spaced at ~16 Hz intervals. The record shows 5–10 Hz changes in the fundamental and harmonic frequencies through time, a phenomenon referred to as gliding. The fundamental frequencies and overtones at times coalesce into broadband energy, implying a change in the boundary conditions of the resonance chamber.

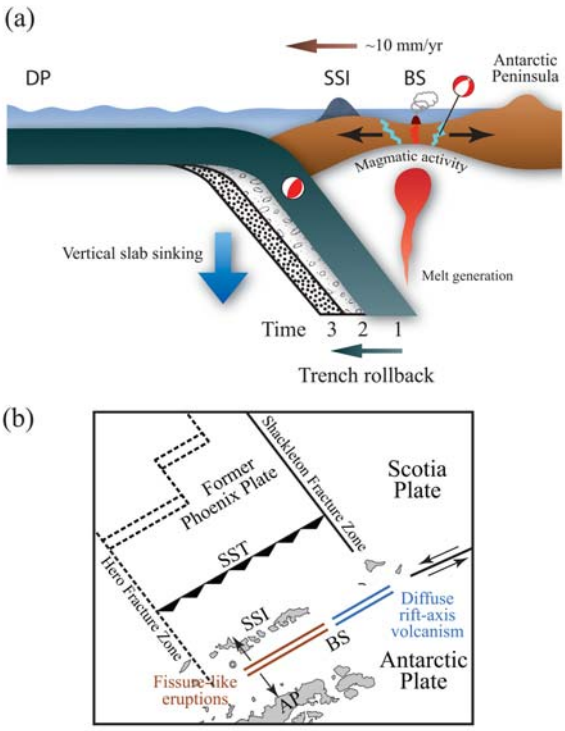

Figure 11. Schematic diagram showing overall tectonic and magmatic processes along the South Shetland Island (SSI) arc, trench and Bransfield Strait (BS) back-arc basin (modified from *Barker and Austin* [1998]) that gave rise to earthquake patterns observed in the hydrophone data. (a) Since active subduction has ceased and the source ridge is extinct, the slab is sinking vertically at the trench and in the upper mantle to move progressively oceanward through time (examples 1, 2, 3). This causes the trench and island arc to move oceanward as well (rollback). This oceanward motion results in continued horizontal extension in the back-arc region. Slab-induced melting and extension in the back arc leads to magmatic and tectonic activity in the Bransfield Strait. Thrust events may still occur within the subducted slab and along the plate interface. (b) The Bransfield is opening though complex rift propagation from northeast to southwest. Extensive rift volcanism in the northeast gives way to more isolated, fissure-like eruptive features in the southwest.

were likely well located compared to background (lower level) seismicity because the swarm earthquakes were larger than background events, thus allowing for earthquakes to be detected on all stations and improving location accuracy. The long-term peaks in background seismicity from December 2005 to March 2006 and December 2006 to October 2007 are also intriguing; however, several more years of data are required to quantify any periodicity to this pattern and allow identification of a possible geophysical cause.

[22] Eight swarms of seismicity were observed along the neovolcanic zone the back arc. All occurred at, or along the flanks of, major volcanic centers, consistent with the events being triggered by intrusive magmatic activity (Figure 8). The swarms occurred at (in temporal order) Hook Ridge, Three Sisters, Edifice-A, Bridgeman Island, Wordie Volcano, Orca Volcano, Three Sisters, and Deception Island. The three earthquake swarms at Edifice-A and Three Sisters show some indication of earthquake migration, which is observed during magma injection events at mid-ocean ridges associated with intrusion, and lateral propagation, of magma into shallow crust [*Einarsson and Brandsdottir*, 1980; *Dziak et al.*, 2007]. However, the earthquake propagation direction is oblique to the strike of the rift zone, and given the location error, the epicenter migration may not be statistically significant. The five other earthquake swarms remained equidistant from the nearest volcanic center during the duration of activity, implying that magma was not injected laterally along the rift zone during these episodes. Yet, the presence of earthquake sequences that exhibit tight space-time clustering and contain many similar magnitudes events does indicate that magma intrusion likely initiated the activity.

[23] The four swarms that occurred over a 3 week period in August 2006 (Figure 8) are distributed over nearly the entire 400 km length of the Bransfield back-arc rift zone, from Deception Island to Wordie Volcano. This August 2006 rifting sequence began with two swarms in the southwest Bransfield back arc that occurred within a 4 day period, while the other two occurred 10 days later and 150 km down rift during August 26–28. Although speculatively these four swarms could be related, it is more likely given the distance separating the two clusters that they were not from one large, Bransfield back-arc-wide, extension event.

[24] A total of 122 hydroacoustic earthquakes were located at the trench, consistent with prior observations that the slab and trench are active earthquake zones. *Robertson-Maurice et al.* [2003] used seismic stations to locate 24 earthquakes along the fore-arc region extending from the South Shetland trench axis toward and beneath the South Shetland Islands, which they interpreted as evidence of a subducted slab along the South Shetland subduction zone. Their seismic depths (generally 10–50 km) and locations of the earthquakes suggest they may represent the shallow thrust faulting events that generally occur along the shallowly dipping thrust interface of subduction zones. Although earthquake focal depth and source parameter information are not available from our hydroacoustic analysis techniques, the large amount of seismicity from the trench and continental shelf is consistent with these previous seismically based interpretations.

[25] In addition, *González-Casado et al.* [2000] argue from teleseismic earthquake data that the Bransfield back arc is opening from sinistral simple shear between the Scotia and Antarctic plates. They invoke the lack of teleseismic earthquakes from the South Shetland Trench to suggest there is no trench rollback, and active extension at the back arc leads to compression at the South Shetland Islands. The hydroacoustic earthquake data presented here indicates earthquakes are likely occurring within the subducted slab or along the trench interface, which is consistent with the rollback model and gravity- driven deformation of the slab as it sinks into the upper mantle. If the interplate interface at the trench is locked and rollback is not occurring, then opening of the Bransfield back-arc basin would be caused by the sinistral Antarctic-Scotia plate motion and deformation of the Shetland Islands (and therefore seismicity) would be occurring over a much broader, distributed zone. Moreover, the large amount of seismicity along the northwestern and southeastern margins of the Bransfield is consistent with the active listric and

detachment normal faulting observed from multichannel seismic data and invoked in the rift propagation trench rollback model [*Barker and Austin*, 1998; *Christeson et al.*, 2003].

[26] Figures 11a and 11b show a summary of the tectonic and magmatic processes (modified from *Barker and Austin* [1998]) that resulted in the earthquake patterns observed in the hydrophone data. Since the Phoenix Ridge is extinct, the slab sinks vertically at the trench and in the upper mantle to move progressively oceanward through time, resulting in migration of the trench and island arc oceanward in response to this rollback (Figure 11a). This oceanward motion results in continued horizontal extension in the back-arc region. Slab-induced melting and extension in the back arc lead to magmatic and tectonic activity in the Bransfield back arc. The Bransfield back arc is opening though complex rift propagation from northeast to southwest (Figure 11b). Extensive rift volcanism in the northeast gives way to more isolated, fissure-like eruptive features in the southwest. Continued propagation of Bransfield back-arc rifting from northeast to southwest represents two main tectonic factors: (1) transtensional tectonics at the complex Scotia-Antarctic triple junction and (2) migration of the slab window to the northeast, enabling rollback to initiate and accelerate along the trench [*Barker and Austin*, 1998].

[27] The icequake locations illustrate the dynamic behavior of sea ice in the Bransfield Strait and Antarctic Peninsula region. The icequakes show a strong seasonal variability in occurrence, reflecting the freeze-thaw cycle with most icequakes being detected during the austral summer months. The lesser histogram peak in icequake activity during the austral winter likely reflects the increase in wind and wave stress rather than the thermal stress that dominates the summer months. The icequake locations southeast of the Bransfield Strait show a clear separation into six lobes that trend toward the Antarctic Peninsula. These lobes are not interpreted as artifacts of the location algorithm, since they are perpendicular to the error surface, exceed location error (Figure 3), and appear to parallel the trends of submarine canyons. Thus we interpret the icequakes as likely being caused by impact of the icebergs with each other as well as with the seafloor as they are calved off the glacier fronts and are channeled along the shallow portions of the canyons toward the open ocean. The majority of the icequakes occur near the Antarctic Peninsula at depths less than the 500 m bathymetric contour, consistent with retreat of the ice fronts from the 400 m ground line since the Last Glacial Maximum. Moreover, although we think the majority of earthquakes along the southeastern margin are due to active fault processes, several earthquakes also locate along the Antarctic Peninsula submarine canyons. This suggests either the trend of these canyons may be fault controlled morphologic features, or that some of the icequakes within the canyons may have been misidentified as earthquakes.

[28] The iceberg tremor signals recorded during this 2 year experiment were all located at or near the current position of iceberg UK213, which is in the central Bransfield Strait. Despite the similarity of the harmonic signals to tremor observed from volcanic activity, the location of the signals confirms the iceberg source. The phenomenon of ''gliding'' observed in the iceberg spectrograms had previously only been documented at seafloor and subaerial volcanoes, and are caused by several factors from magma degassing to eruption of lava from the magma chamber. However, in deep-ocean icebergs it is likely due to changes in the length and shape of the boundaries of the water-ice resonance chamber within the iceberg, probably from frictional heating and/or abrasion as the iceberg scrapes along the seafloor. The fundamental frequency from the UK213 iceberg implies a signal source size of between 29.8 and 37.3 m at a 1490 m s^{-1} mean sound velocity. Since the iceberg is ~10 km in length and is likely several times thicker than the ~300 m high section of iceberg exposed above the sea surface, this suggests the harmonic tremor is produced by resonance of a small chamber or pocket of fluid within the iceberg rather than by resonance of the entire berg itself. The fundamental frequencies and overtones of the signals at times coalesce into broadband energy, implying a change in the boundary conditions of the resonance chamber. Alternatively, as suggested by *MacAyeal et al.* [2008], the iceberg tremor and gliding phenomena could be due to periodicity of discrete stick-slip events caused by contact of the moving iceberg with the seafloor rather than resonant vibration. This explanation is preferred since it implies the tremor fundamental and overtone frequencies are a direct function of the size of the ice-seafloor contact and the speed of the iceberg, rather than requiring a change in sound speed or dimensions of a zone of resonance within the iceberg.

[29] Analysis of the hydroacoustic data presented here has provided further perspective on the various models of back-arc extension and otherwise unknown active volcanic processes of the Bransfield Strait seafloor. Inclusion of cryogenic signals provides a climatic perspective, and elucidates the multiple geophysical forces shaping seafloor morphology as well as the multifaceted nature of the ocean sound field in this complex tectonovolcanic basin. To understand better the relative contribution of earthquakes and icequakes to the overall ocean conditions in the Bransfield Strait, we estimated the total energy release of each phenomenon. The total acoustic energy release from earthquakes and icequakes in the Bransfield Strait water column can be estimated by converting source level to seismic magnitude (described in section 3), then to energy E using the equation $\mathrm{Log}(E) = 5.8 + 2.4\ m_b$ [*Kasahara*, 1981]. This yields the result that total icequake energy release (1.9×10^{17} ergs) exceeds total earthquake acoustic energy (1.1×10^{17} ergs) by roughly a factor of 2. Since these 2 year energy estimates represent the combined release of mechanical energy, acoustic wave energy and heat, these totals demonstrate the significant role ice breakup has not only on the ocean sound field, but also on the physical oceanographic conditions within the Bransfield Strait.

6. Summary

[30] Despite the lack of a deep-water sound channel within the water column of Bransfield Strait, hydroacoustic monitoring techniques provided useful information on the seismic activity of seafloor volcanic and tectonic features as well as on the long-term patterns of ice breakup in the region. The major results of our study are summarized as follows:

[31] 1. From 2005 to 2007, our moored hydrophone array detected 3,900 earthquakes, 5,925 icequakes and numerous

ice tremor events from throughout the Bransfield Strait, South Shetland Island, and South Shetland Trench.

[32] 2. A total of eight swarms of seismicity were observed along the neovolcanic zone and the back arc. All occurred at, or along the flanks of, major volcanic centers, consistent with the events being triggered by intrusive magmatic activity.

[33] 3. The presence of earthquakes along the trench and subducted slab is consistent with the rollback model and gravity-driven deformation of the slab as it sinks into the upper mantle.

[34] 4. The icequakes show a temporal pattern related to seasonal freeze-thaw cycles and a spatial distribution consistent with channeling of sea ice along submarine canyons from glacier fronts.

[35] 5. Harmonic tremor was detected from a large ($\sim$30 km^2) iceberg in the northeast Bransfield Strait. These signals are likely due to resonance of small (29–37 m) fluid chamber or cavity within iceberg, rather than by resonance of the entire berg.

[36] **Acknowledgments.** The authors thank the captain and crew of the R/V *Yuzhmorgeologiya* and the captain and personnel of King Sejong Base, King George Island, Antarctica, for their support during staging and deployment of the hydrophone arrays. The authors also wish to thank B. Hanshumaker, T.-K. Lau, K. Stafford, S. Heimlich, M. Fowler, A. Young, and S. Yun for their at sea support and laboratory assistance. The authors owe special thanks to J.-H. Lee for his hard work during the first successful deployment/recovery in Antarctic waters, without which the hydrophone experiment could not begin. Also thanks to J. Hong for providing additional ship time during the hydrophone deployments and D. Mellinger for providing the Ishmael software. This project was made possible through support of the Korea Ocean and Polar Research Institute and the NOAA Ocean Exploration Program, PMEL contribution 3265, and KOPRI projects PP08020 and PM09030.

References

Banfield, L. A., and J. B. Anderson (1995), Seismic facies investigation of late Quaternary glacial history of Bransfield Basin, Antarctica, in *Geology and Seismic Stratigraphy of the Antarctic Margin*, *Antarct. Res. Ser.*, vol. 68, edited by A. K. Cooper, P. F. Barker, and G. Brancolini, pp. 123–140, AGU, Washington, D. C.

Barker, D. H. N., and J. A. Austin (1998), Rift propagation, detachment faulting, and associated magmatism in Bransfield Strait, Antarctic Peninsula, *J. Geophys. Res.*, *103*(B10), 24,017–24,043, doi:10.1029/98JB01117.

Barker, D. H., et al. (2003), Backarc basin evolution and cordilleran orogenesis: Insights from new ocean-bottom seismograph refraction profiling in Bransfield Strait, Antarctica, *Geology*, *31*, 107–110, doi:10.1130/0091-7613(2003)031<0107:BBEACO>2.0.CO;2.

Bevington, P. R., and D. K. Robinson (1992), *Data Reduction and Error Analysis for the Physical Sciences*, chap. 11, McGraw-Hill, New York.

Bevis, M., et al. (1999), GPS studies of geodynamics in the Scotia Arc and West Antarctica, paper presented at 8th International Symposium on Antarctic Earth Sciences, Sci. Comm. on Antarct. Res., Wellington, New Zealand.

Canals, M., R. Urgeles, and A. M. Calafat (2000), Deep sea-floor evidence of past ice streams off the Antarctic Peninsula, *Geology*, *28*(1), 31–34, doi:10.1130/0091-7613(2000)028<0031:DSEOPI>2.0.CO;2.

Canals, M., J. L. Casamor, R. Urgeles, A. M. Calafat, E. W. Domack, J. Baraza, M. Farran, and M. De Batist (2002), Seafloor evidence of a subglacial sedimentary system off the northern Antarctic Peninsula, *Geology*, *30*, 603–606, doi:10.1130/0091-7613(2002)030<0603:SEOASS>2.0.CO;2.

Chapp, E., D. R. Bohnenstiehl, and M. Tolstoy (2005), Sound-channel observations of ice-generated tremor in the Indian Ocean, *Geochem. Geophys. Geosyst.*, *6*, Q06003, doi:10.1029/2004GC000889.

Christeson, G. L., D. H. N. Barker, J. A. Austin Jr., and I. W. D. Dalziel (2003), Deep crustal structure of Bransfield Strait: Initiation of a back arc basin by rift reactivation and propagation, *J. Geophys. Res.*, *108*(B10), 2492, doi:10.1029/2003JB002468.

Davis, T. M., K. A. Countryman, and M. J. Carron (1986), Tailored acoustic products utilizing the NAVOCEANO GDEM (a generalized digital environmental model), paper presented at 36th Naval Symposium on Underwater Acoustics, Nav. Ocean Syst. Cent., San Diego, Calif.

Dietrich, R., et al. (2001), ITRF coordinates and plate velocities from repeated GPS campaigns in Antarctica—An analysis based on different individual solutions, *J. Geod.*, *74*, 756–766, doi:10.1007/s001900000147.

Dushaw, B., and J. A. Colosi (1998), Ray tracing for acoustic tomography, *Rep. APL-U W TM 3-98*, Appl. Phys. Lab., Univ. of Wash., Seattle, Dec.

Dziak, R. P. (2001), Empirical relationship of T-wave energy and fault parameters of northeast Pacific Ocean earthquakes, *Geophys. Res. Lett.*, *28*, 2537–2540, doi:10.1029/2001GL012939.

Dziak, R. P., D. R. Bohnenstiehl, H. Matsumoto, C. G. Fox, D. K. Smith, M. Tolstoy, T.-K. Lau, J. Haxel, and M. J. Fowler (2004), P- and T- wave detection thresholds, Pn velocity estimate, and detection of lower mantle and core P waves on ocean sound-channel hydrophones at the Mid-Atlantic Ridge, *Bull. Seismol. Soc. Am.*, *94*(2), 665–677, doi:10.1785/0120030156.

Dziak, R. P., D. R. Bohnenstiehl, J. P. Cowen, E. T. Baker, K. H. Rubin, J. H. Haxel, and M. J. Fowler (2007), Rapid dike injection leads to volcanic eruptions and hydrothermal plume release during seafloor spreading events, *Geology*, *35*, 579–582, doi:10.1130/G23476A.1.

Einarsson, P., and B. Brandsdottir (1980), Seismological evidence for lateral magma intrusion during the July 1978 deflation of Krafla Voclano in NE Iceland, *J. Geophys. Res.*, *47*, 160–165.

Garces, M. A., M. T. Hagerty, and S. Y. Schwartz (1998), Magma acoustics and time-varying melt properties at Arenal Volcano, Costa Rica, *Geophys. Res. Lett.*, *25*, 2293–2296, doi:10.1029/98GL01511.

González-Casado, J. M., J. L. Giner-Robles, and J. Lopez-Martinez (2000), Bransfield Basin, Antarctic Peninsula: Not a normal backarc basin, *Geology*, *28*, 1043–1046, doi:10.1130/0091-7613(2000)28<1043:BBAPNA>2.0.CO;2.

Gràcia, E., M. Canals, M.-L. Farran, J. Sorribas, and R. Pallas (1997), Central and eastern Bransfield basins (Antarctica) from high-resolution swath-bathymetry data, *Antarct. Sci.*, *9*, 168–180, doi:10.1017/S0954102097000229.

Grad, M., A. Guterch, and P. Sroda (1992), Upper crustal structure of Deception Island area, Bransfield Strait, West Antarctica, *Antarct. Sci.*, *4*, 469–476, doi:10.1017/S0954102092000683.

Grad, M., H. Shiobara, T. Janik, A. Guterch, and H. Shimamura (1997), Crustal model of the Bransfield Rift, West Antarctica, from detailed OBS refraction experiments, *Geophys. J. Int.*, *130*, 506–518, doi:10.1111/j.1365-246X.1997.tb05665.x.

Kasahara, K. (1981), *Earthquake Mechanics*, 248 pp., Univ. of Cambridge, Cambridge, U. K.

Keller, R. A., M. R. Fisk, J. L. Smellie, J. A. Strelin, and L. A. Lawver (2002), Geochemistry of back arc basin volcanism in Bransfield Strait, Antarctica: Subducted contributions and along-axis variations, *J. Geophys. Res.*, *107*(B8), 2171, doi:10.1029/2001JB000444.

Klinkhammer, G. P., C. S. Chin, R. A. Keller, and A. Dahlmann (2001), Discovery of new hydrothermal vent sites in the Bransfield Strait, Antarctica, *Earth Planet. Sci. Lett.*, *193*, 395–407, doi:10.1016/S0012-821X (01)00536-2.

Lawver, L. A., et al. (1996), Distributed active extension in Bransfield Basin, Antarctic Peninsula: Evidence from multibeam bathymetry, *GSA Today*, *6*(11), 1–6.

MacAyeal, D. R., E. A. Okal, R. C. Aster, and J. N. Bassis (2008), Seismic and hydroacoustic tremor generated by colliding icebergs, *J. Geophys. Res.*, *113*, F03011, doi:10.1029/2008JF001005.

Maestro, A., L. Somoza, J. Rey, J. Martinez-Frias, and J. Lopez-Martinez (2007), Active tectonics, fault patterns, and stress field of Deception Island: A response to oblique convergence between the Pacific and Antarctic plates, *J. South Am. Earth Sci.*, *23*, 256–268, doi:10.1016/j.jsames.2006.09.023.

Matsumoto, K., T. Sato, T. Takanezawa, and M. Ooe (2001), GOTIC2: A program for computation of oceanic tidal loading effect, *J. Geod. Soc. Jpn.*, *47*, 243–248.

Prieto, M. J., M. Canals, G. Ercilla, and M. de Batist (1998), 1998, Structure and geodynamic evolution of the central Bransfield Basin (NW Antarctica) from seismic reflection data, *Mar. Geol.*, *149*, 17–38, doi:10.1016/S0025-3227(98)00038-3.

Robertson-Maurice, S. D., D. A. Wiens, P. J. Shore, E. Vera, and L. M. Dorman (2003), Seismicity and tectonics of the south Shetland Islands and Bransfield Strait from a regional broadband seismograph deployment, *J. Geophys. Res.*, *108*(B10), 2461, doi:10.1029/2003JB002416.

Sandwell, D. T., and W. H. F. Smith (1997), Marine gravity anomaly from Geosat and ERS 1 satellite altimetry, *J. Geophys. Res.*, *102*(B5), 10,039–10,054, doi:10.1029/96JB03223.

Slack, P. D., C. G. Fox, and R. P. Dziak (1999), P wave detection thresholds, Pn velocity estimates, and T wave location uncertainty from oceanic hydrophones, *J. Geophys. Res.*, *104*(B6), 13,061–13,072, doi:10.1029/1999JB900112.

Stroup, D. F., D. R. Bohnenstiehl, M. Tolstoy, F. Waldhauser, and R. T. Weekly (2007), Tidal triggering of microearthquakes at 9°50′N East Pacific Rise, *Geophys. Res. Lett.*, *34*, L15301, doi:10.1029/2007GL030088.

Talandier, J., O. Hyvernaud, E. A. Okal, and P.-F. Piserchia (2002), Long-range detection of hydroacoustic signals from large icebergs in the Ross Sea, Antarctica, *Earth Planet. Sci. Lett.*, *203*, 519–534, doi:10.1016/S0012-821X (02)00867-1.

Taylor, B., A. M. Goodliffe, and F. Martinez (1999), How continents break up: Insight from Papua New Guinea, *J. Geophys. Res.*, *104*(B4), 7497–7512, doi:10.1029/1998JB900115.

Tolstoy, M., F. L. Vernon, J. A. Orcutt, and F. K. Wyatt (2002), The breathing of the seafloor: Tidal correlations of seismicity on Axial volcano, *Geology*, *30*, 503–506, doi:10.1130/0091-7613(2002)030<0503:BOTSTC>2.0.CO;2.

Wilcock, W. S. D. (2001), Tidal triggering of microearthquakes on the Juan de Fuca Ridge, *Geophys. Res. Lett.*, *28*, 3999–4002, doi:10.1029/2001GL013370.

D. R. Bohnenstiehl, Department of Marine, Earth and Atmospheric Sciences, North Carolina State University, Raleigh, NC 27695-8208, USA.

R. P. Dziak, J. H. Haxel, and H. Matsumoto, Cooperative Institute for Marine Resources Studies, Oregon State University, NOAA Newport, OR 97365-5258, USA.

W. S. Lee and M. Park, Polar Environmental Research Division, Korea Polar Research Institute, Incheon 406-840, South Korea.